Damage characterization of high-strength multiphase steels

S Heibel[1], W Nester[1], T Clausmeyer[2] and A E Tekkaya[2]

[1] Daimler AG, Benzstraße, 71059 Sindelfingen, Germany
[2] Institute of Forming Technology and Lightweight Design, TU Dortmund University, Baroper Str. 303, 44227 Dortmund, Germany

E-mail: sebastian.heibel@daimler.com

Abstract. High-strength steels show an entirely different material behavior than conventional deep-drawing steels. This fact is caused among others by the multiphase nature of their structure. The Forming Limit Diagram as the classic failure criterion in forming simulation is only partially suitable for this class of steels. An improvement of the failure prediction can be obtained by using damage mechanics. Therefore, an exact knowledge of the material-specific damage is essential for the application of various damage models. In this paper the results of microstructure analysis of a dual-phase steel and a complex-phase steel with a tensile strength of 1000 MPa are shown comparatively at various stress conditions. The objective is to characterize the basic damage mechanisms and based on this to assess the crack sensitivity of both steels. First a structural analysis with regard to non-metallic inclusions, the microstructural morphology, phase identification and the difference in microhardness between the structural phases is carried out. Subsequently, the development of the microstructure at different stress states between uniaxial and biaxial tension is examined. The damage behavior is characterized and quantified by the increase in void density, void size and the quantity of voids. The dominant damage mechanism of the dual-phase steel is the void initiation at phase boundaries, within harder structural phases and at inclusions. In contrast the complex-phase steel shows a significant growth of a smaller amount of voids which initiate only at inclusions. To quantify the damage tolerance and the susceptibility of cracking the criterion of the fracture forming limit line (FFL) is used. The respective statements are supported by results of investigations regarding the edge-crack sensitivity.

1. Introduction

The classic tool for failure prediction in metal forming is the forming limit diagram. With this tool the beginning of localized necking can be determined. In nowadays car body design less ductile, high strength materials are used for safety-relevant structural components. For these materials the use of the forming limit diagram is considered to be problematic: For example the failure in the plane-strain region is predicted too early with the forming limit curve, thus the material capacity is underestimated [1]. Another example is the inability of displaying edge cracks correctly. This can be remedied by damage mechanics. Micromechanical motivated damage models for example try to model the damage development that occurs with ductile fracture from void nucleation, growth and coalescence to the initiations of microcracks [2]. These effects are particularly favored by the multiphase nature of high strength steels as has been shown in various studies for dual phase steels [3], [4]. The different formability of the respective phases leads to an inhomogeneous distribution of deformation. Voids develop on the boundary of different phases or within the more brittle phase. If the martensite is finely dispersed in the microstructure, more ferrite is deformed and there are fewer nucleation sites for

damage initiation. In [3] it was found that inclusions with an elongated shape rather break, whereas globulistic forms dissolve from the matrix. Furthermore, it was shown that the porosity increases with increasing hardness gradient within a material. In addition, the band-type formation of a second phase favors the void nucleation. Larger martensite clusters can lead to significant damage accumulation, since only a small proportion of ferrite may be deformed. Referring to different stress states Tasan et al. could prove that increasing stress triaxiality leads to an earlier onset of void nucleation and equally increases the void density in dual-phase steels [4]. The mentioned triaxiality is often used for the description of the void growth in damage mechanics [5]. Based on this and taking into account the independence of the thickness of the fracture surface from stress state and stress history Martins et al. developed the concept of fracture forming limit curves [6], [7]. Because of the constant critical thickness reduction the critical damage parameter derived from the fracture forming line can be considered as a material parameter. This parameter is used here to quantify the damage tolerance. In addition to the low damage tolerance the edge-crack sensitivity could be a problem by the application of dual-phase steels in industrial practice. By shear cutting operations during manufacturing the formability at the shear-cut-edge is reduced. The reasons for this purpose lie like the causes for damage evolution in the microstructure of the material. A small grain size, a homogeneous structure, the absence of microstructure stringers or bands as well as the minimization of inclusions have a positive effect on the edge-crack sensitivity. To evaluate the edge-crack sensitivity the edge-fracture-tensile-test developed by Feistle et al. shows promising results [8]. With the help of this test, the statements on damage tolerance should be supported in this work.

2. Materials

Dual- and complex-phase steels exhibit a completely different macroscopic material behavior because of their different microstructural characteristics. Dual-phase steels have traditionally a ferritic matrix containing martensite at the grain boundaries, whereas complex-phase steels are characterized by a bainitic microstructure. Other structural phases in a conventional complex-phase steel are ferrite and a smaller amount of martensite. Table 1 shows the volume fraction of phases of the examined materials with a nominal sheet thickness of 1 mm.

Table 1. Volume fraction of phases

	DP1000	CP1000
Ferrite	27.3 %	4.6 %
Bainite/ tempered martensite	59.5 %	93.5 %
Martensite	9.5 %	0.5 %
Retained austenite	2.3 %	0.3 %

The dominant phases of the dual-phase steel (DP1000) are ferrite and bainite. In addition to martensite a small amount of retained austenite is included in the structure. The structure of the complex-phase steel (CP1000) with the volume fractions shown in table 1 corresponds to the classical composition. According to the identified microstructural phases, the dual-phase steel exhibit with 546 HV a significantly greater difference in microhardness than the complex-phase steel with 385 HV. In figure 1, the very fine-grained microstructure of both materials is illustrated by the nital etching in longitudinal section.

For the dual-phase steel a significant amount of stringers and bands could be seen. The phases of the complex-phase steel are very homogeneously distributed, which confirms the right illustration of figure 1. In addition a larger number of titanium carbides can be determined by an energy-dispersive X-ray spectroscopy (EDX) for the complex-phase steel. These brittle inclusions provide a nucleation site to damage development.

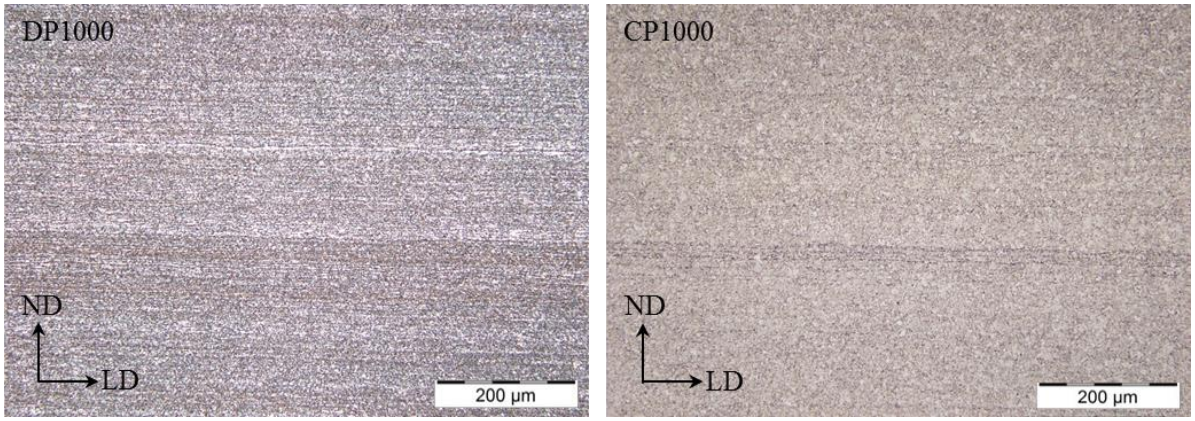

Figure 1. Microstructure after nital etching

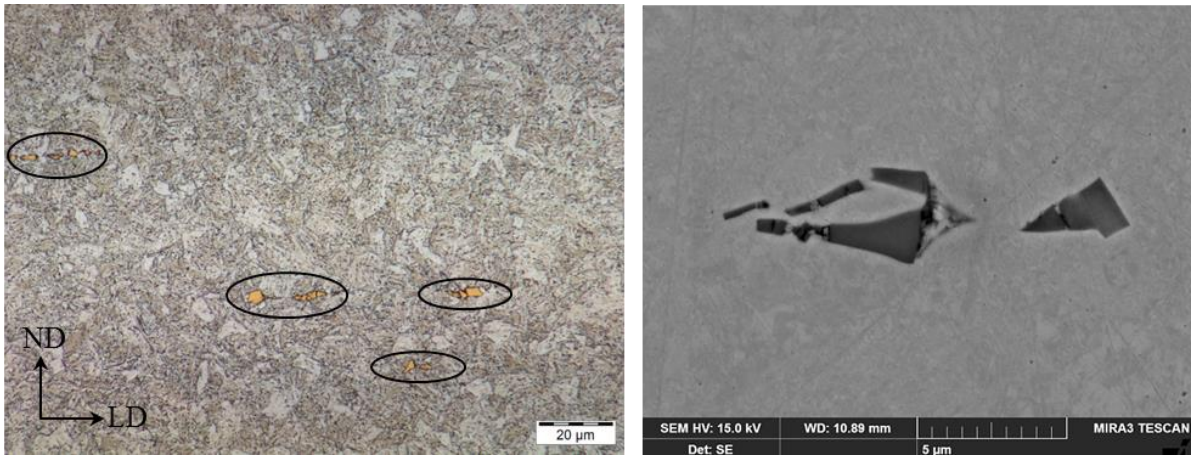

Figure 2. Titanium carbides in the microstructure of CP1000

Besides of the titanium carbides aluminum oxide inclusions can be identified in the structure. These aluminum oxides are likewise present in the dual-phase steel. Moreover softer manganese sulfides can be found here. Table 2 summarizes the mechanical properties of these two steels. The lower yield ratio results from the microstructural composition of the DP1000 and thus results in a relatively high global formability at a strength of 1000 MPa.

Table 2. Mechanical Properties (longitudinal direction)

Material	$R_{p0,2}$ [MPa]	R_m [MPa]	$R_{p0,2}/R_m$ [-]	A_G [%]	A_{80} [%]	n [-]	r_0 [-]	r_{45} [-]	r_{90} [-]	r_m [-]
DP1000	675	1035	0.652	9	13	0.129	0.715	1.088	0.918	0.952
CP1000	903	1012	0.892	5	7	0.053	0.990	1.235	1.080	1.135

The bainitic microstructure of the CP1000 leads, among others due to the smaller difference in hardness between the phases, to an excellent local formability. Both materials have no pronounced normal anisotropy.

3. Experimental methodology

To characterize the damage behavior at different stress states four specimens are used as shown in Figure 3 and 4. For the uniaxial tension (UAT) a classical tensile test specimen according to EN ISO 6892-1 and a smaller one in size is used. The stress state of the plane-strain tension (PST) is obtained by a notched tensile specimen with a notch radius of 4 mm.

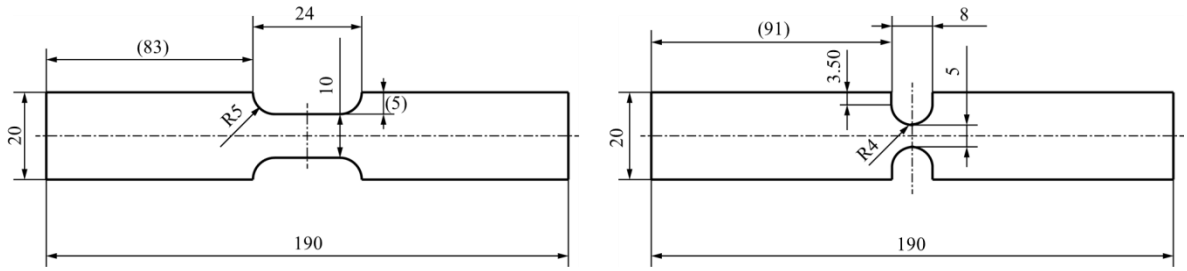

Figure 3. Technical drawing of the smaller in size uniaxial tension specimen (left) and of the plane-strain tension specimen (right)

With regard to damage characterization in the equi-biaxial tensile region (BAT) a cruxiform specimen is unsuitable due to their inhomogeneous strain and stress field. Instead a Nakajima-geometry with a diameter of 200 mm according to EN ISO 12004-2 is used.

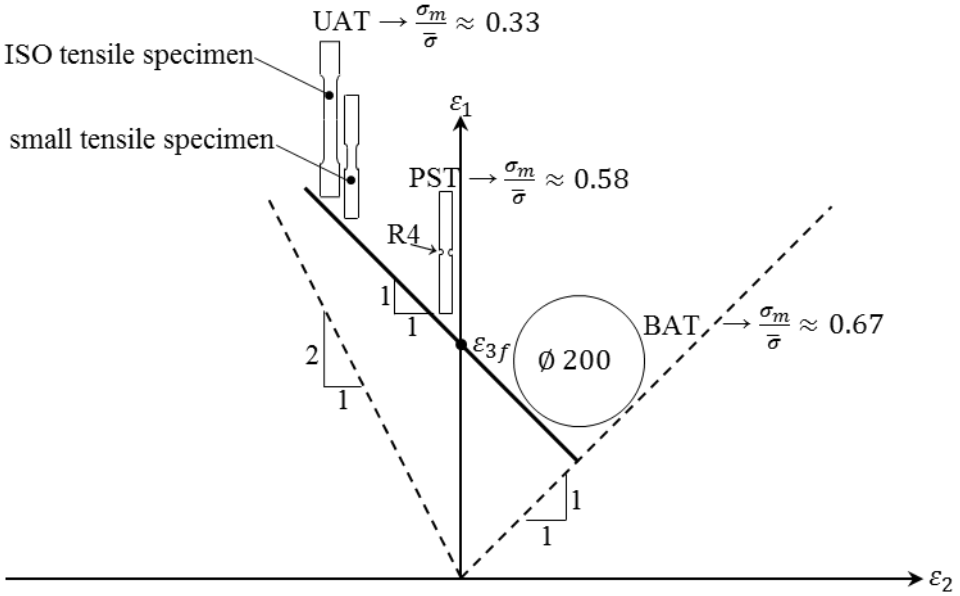

Figure 4. Concept of fracture forming line (FFL) and used specimens [6], [7]

After performing the appropriate quasi-static tensile tests in the longitudinal direction up to fracture, they are stopped at the crosshead displacement of occurrence of maximum force, F_{max}, as well as at 50%, 75%, 85%, 90% and 95% of crosshead displacement at fracture. Instead of test termination at F_{max} the Nakajima-test is stopped at a stamp displacement of 99%. For each stress state and each load level the microstructure is examined with the help of light microscopy, scanning electron microscopy and EDX. To determine the FFL, the thickness reduction is measured at the fractured samples in order to calculate the third principal strain at fracture ε_{3f}. Due to the independence of ε_{3f} of the stress state and the loading history the FFL has a slope of -1 [6], [7]:

$$\varepsilon_{1f} + \varepsilon_{2f} = -\varepsilon_{3f} \approx \text{const.} \tag{1}$$

To quantify the damage tolerance the damage parameter D_{crit} is used [6], [7]:

$$D_{crit} = \int_0^{\bar{\varepsilon}_f} \frac{\sigma_m}{\bar{\sigma}} d\bar{\varepsilon} = -\frac{(1+r_m)}{3} \varepsilon_{3f} \tag{2}$$

This characteristic value is motivated by the damage mechanics in the form of effective strain fracture criteria and its weighting function, the stress triaxiality $\sigma_m/\bar{\sigma}$, which is defined as the ratio of the hydrostatic stress σ_m and the effective stress $\bar{\sigma}$. Further, the anisotropic yield criterion Hill48 was

used for the definition by Martins [6], [7]. To support the statement of damage tolerance with edge-crack sensitivity results the edge-fracture-tensile-test developed and executed at the Institute of Metal Forming and Casting (utg) is used for both materials. For this purpose a tensile test (UAT) is performed with both edges milled as wells as one side milled and one shear cut edge. The sample with both edges milled shows a classic ductile failure in the center of the specimen whereas the formability of the shear cut edge is reduced by the stamping process and an edge crack is initiated. This reduced formability is recorded with a digital image correlation system [8].

4. Results and discussion

Firstly the damage initiation mechanisms of both materials are worked out. Based on this the damage evolution is represented comparatively in different stress states. Finally, the damage tolerance of the examined materials is characterized.

4.1. Damage initiation

In the examined DP1000 several damage nucleation sites can be found. In figure 5 the void nucleation by fracture of a manganese sulfide is illustrated.

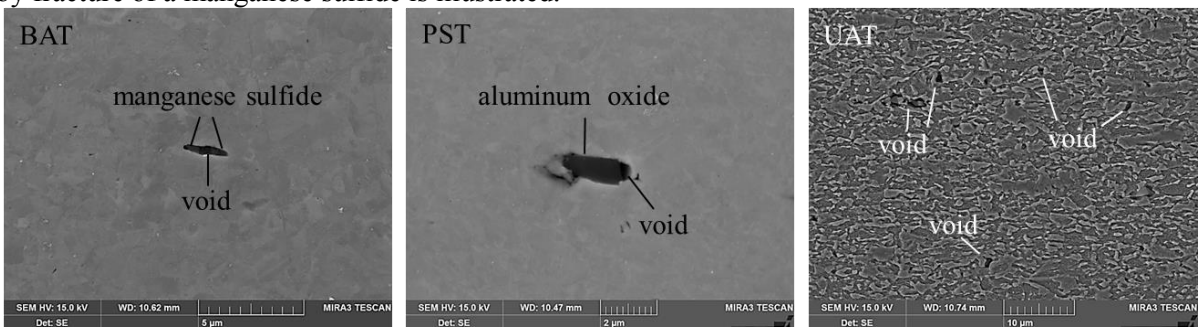

Figure 5. Damage initiation DP1000

Furthermore, voids are formed by decohesion of the matrix from aluminum oxide inclusions. As can be seen in the right illustration of figure 5, the voids also nucleate at the phase boundaries between martensite and ferrite. This effect could be favored by the difference in hardness between the two phases. Due to the brittleness of the martensite, fracture occurs on the very same. These observations correspond to the work of Tasan et al., who showed for a dual-phase steel damage initiation by particle-matrix decohesion, particle cracking, martensite fracture and phase boundary decohesion [4]. The complex-phase steel hardly shows the latter effects of damage initiation as result of the multiphase nature of high-strength steels.

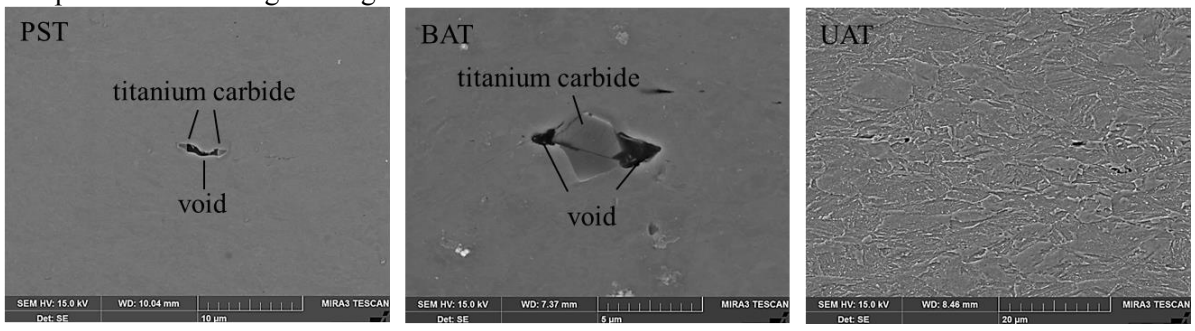

Figure 6. Damage initiation CP1000

The damage initiation is clearly visible here only at inclusions. In figure 6 the void initiation is shown by fractured, brittle titanium carbides. In addition, it comes to decohesion from the matrix. The common occurrence of particle cracking and particle-matrix decohesion could be explained by the high stress triaxiality in the region of BAT. Furthermore, damage initiation for the complex-phase steel is also recorded at aluminum oxide inclusions.

4.2. Damage mechanisms

To assess the damage mechanisms, the porosity, the number of voids and their maximum size are determined by gray-scale analysis in light microscope images of longitudinal cuts of the specimens in a representative region of interest at the respective stress state and load level. Thereby the minimum detectable void size is about 0.305 µm. Table 3 summarizes the results. The dual-phase steel shows an increase in damage accumulation in terms of porosity from UAT through the PST to BAT. Both, the measured quantity as well as the maximum size of the voids increases with rising second principal strain. The complex-phase steel shows a different behavior. No differences between the stress states can be observed. For the UAT the porosity is nearly at a similar level as in the dual-phase steel and therefore lower in the investigated stress states with higher stress triaxiality. In both materials the damage accumulation increases accompanied by a sharply increasing localization.

Table 3. Porosity, size of voids, quantity of voids

		DP1000				CP1000		
		Porosity [%]	Quantity	Max. size [µm]		Porosity [%]	Quantity	Max.size [µm]
	F_{max}	-	-	-	F_{max}	-	-	-
	50 %	-	-	-	50 %	-	-	-
	75 %	< 0.01	19	3.12	75 %	-	-	-
UAT	85 %	0.010	53	5.09	85 %	0.01	19	3.48
	90 %	0.067	147	5.85	90 %	0.034	18	14.09
	95 %	0.095	172	6.78	95 %	0.049	44	14.12
	fracture	0.098	159	7.33	fracture	0.108	43	15.17
	F_{max}	0.017	38	4.3	F_{max}	< 0.01	12	3.7
	50 %	-	-	-	50 %	-	-	-
	75 %	0.030	35	5.09	75 %	< 0.01	16	3.96
PST	85 %	0.053	53	6.14	85 %	0.028	25	8.52
	90 %	0.065	80	6.99	90 %	0.056	35	14.11
	95 %	0.138	142	7.08	95 %	0.090	7	11.66
	fracture	0.172	239	9.2	fracture	0.116	49	15.54
	50 %	0.040	4	7.85	50 %	0.010	7	3.45
	75 %	0.050	5	9.14	75 %	0.030	24	3.96
	85 %	0.120	15	8.13	85 %	0.040	16	4.04
BAT	90 %	0.150	199	6.73	90 %	0.060	12	9.44
	95 %	0.160	175	9.8	95 %	0.080	21	11.87
	99 %	0.320	234	13.28	99 %	0.140	35	15.74
	fracture	0.413	486	14.01	fracture	0.153	41	16.7

Figure 7 shows a fractured Nakajima specimen of DP1000. Compared to CP1000 in Figure 8, one recognizes the significantly larger number of voids. Furthermore, the effect of void coalescence can clearly be seen in Figure 7.

Larger voids can be detected in Figure 8 for the CP steel. Besides a micrograph of notched tensile specimen at the load case of 95 % is shown in Figure 8. The significant localization of the material can be seen here. This is accompanied by the development of a large cavity in the interior of the sample. This cavity develops over several load steps and does not lead to sudden failure. The material behaves in a certain way "tough", hence highly damage tolerant.

Figure 7. Damage mechanisms DP1000

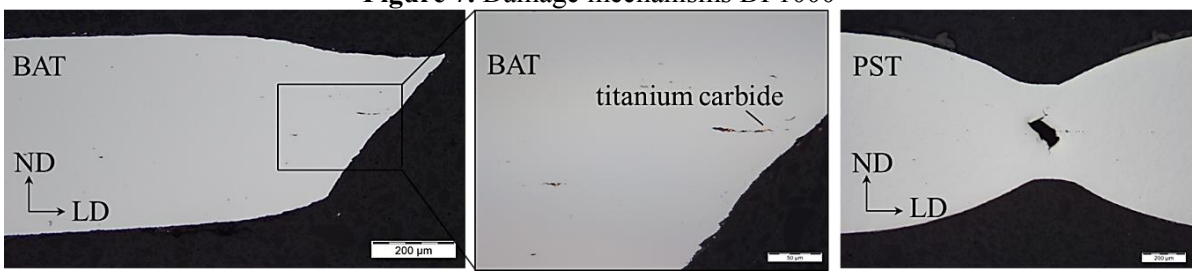

Figure 8. Damage mechanisms CP1000

4.3. Damage tolerance

In the previous sections it was shown that both materials run through the classic stages of ductile damage evolution. Since the concept of FFL is damage mechanically motivated the fracture forming line can be created for both materials according to [6]. Therefore the third principal strain at fracture ε_{3f} must be determined by measuring the fracture thickness for all specimens. The third principal strain at fracture for the DP1000 is -0.514 with a standard deviation of 0.082. ε_{3f} of the CP1000 is amounted -1.114 with a standard deviation of 0.021. The second principal strain is determined via an Aramis 5M digital image correlation system with a strain reference length of 0.5 mm and a frame rate of 2 Hz. Using this second principal strain and the assumption of constant volume, the fracture forming line shown in Figure 9 can be constructed. The slopes of approximately -0.96 for the CP1000 is in accordance with the in [6] developed theory. The slope of the dual-phase steel lies in good agreement with the in [6] and [7] investigated aluminum alloy AA1050-H111.

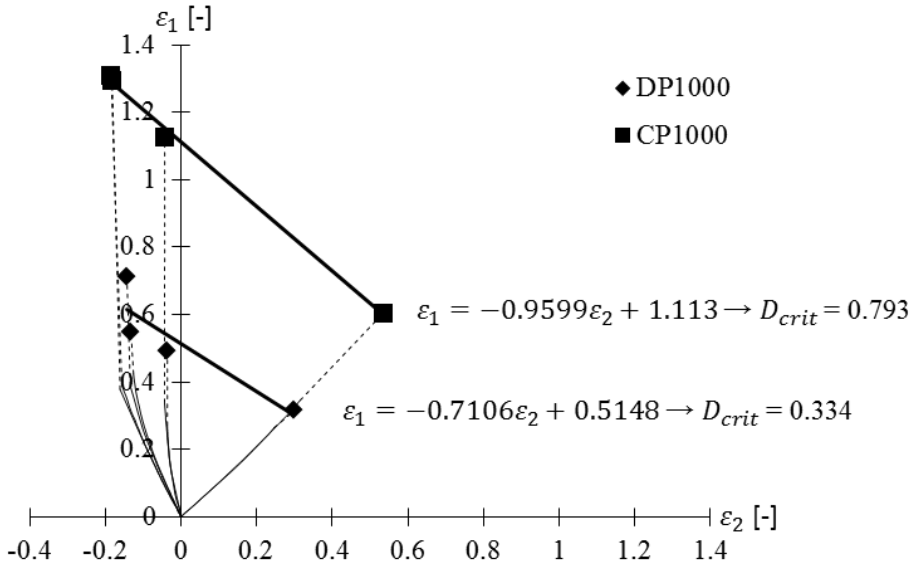

Figure 9. Forming fracture lines with respective loading paths for DP1000 and CP1000

With the third principal strain at fracture and the mean normal anisotropy the critical damage parameter can be determined with equation (2). D_{crit} is determined as 0.793 for the more damage tolerant complex-phase steel more than twice as large as for the dual-phase steel. These results are supported by the results of the edge-fracture-tensile-test [8]. As in table 4 shown for the complex-phase virtually no reduction in the first principal strain can be observed, whereas the dual-phase steel shows significant edge-crack sensitivity with a reduction of first principal strain at fracture of 34%.

Table 4. Results of edge-fracture-tensile-test

	DP1000	CP1000
ε_{1f} at milled cut edge	0.415	0.478
ε_{1f} at milled cut + shear cut edge	0.278	0.453
reduction of ε_{1f}	34 %	5 %

5. Conclusion

The basic damage mechanisms were characterized for both materials. The dual-phase steel as well as the complex-phase steel show regardless of the stress state the mechanisms of ductile damage, namely void initiation, void growth and void coalescence. The voids are nucleated in the dual-phase steel by particle-matrix decohesion, particle cracking, martensite fracture and phase boundary decohesion. Due to the homogeneous, fine-grained bainitic microstructure and the associated low difference in hardness the complex-phase steel shows no damage initiation due to its multiphase nature. Furthermore, the damage accumulation in terms of porosity is independent of the stress state for the complex-phase steel. For the dual-phase steel the damage accumulation increases with increasing second principal strain. For both materials the theory of FFL was confirmed. Using the critical damage parameter, the complex-phase steel could be characterized as damage tolerant and less susceptible to cracking. This statement was supported by the studies on the edge-crack sensitivity for both materials.

Acknowledgements

The authors gratefully acknowledge the experimental support of Martin Kieslich during his employment for the Daimler AG.

References

[1] Till E T, Berger E and Larour P 2008 On an exceptional forming behaviour aspect of ahhs sheets *IDDRG 2008 Int. Conf. (Olofström)* pp 429-440

[2] Gurson A 1977 Continuum theory of ductile rupture by void nucleation and growth: part I-yield criteria and flow rules for porous ductile media *J. Eng. Mat. Tec.* **99** pp 2-15

[3] Pichler A, Tragl E, Kurz T, Werner E, Tsipouridis P, Haglund A, Zajac J, Artimez J M and Ferreno J 2009 *DP grades with improved formability* (Brussels: European Comission Research Fund for Coal and Steels Unit)

[4] Tasan C C, Hoefnagels J P M, ten Horn C H I J and Geers M G D 2009 Experimental analysis of strain path dependent ductile damage mechanics and forming limits *Mech. Mat.* **41** pp 1264-76

[5] McClintock F A 1968 A criterion for ductile fracture by the growth of holes *J. Appl. Mech.* 35 pp 343-71

[6] Martins P A F, Bay N, Tekkaya A E and Atkins A G 2014 Characterization of fracture loci in metal forming *Int. J. Mech. Sci.* **83** pp 112-23

[7] Isik K, Silva M B, Tekkya A E and Martins P A F 2014 Formability limits by fracture in sheet metal forming *J. Mat. Pro. Tec.* **214** pp 1557-65

[8] Feistle M, Krinninger M, Pätzold I and Volk W 2015 Edge-Fracture-Tensile-Test *60 Excellent Inventions in Metal Forming* ed Tekkaya A E, Brosius A and Homberg W (Berlin Heidelberg: Springer-Verlag) pp 193-8